Some issues concerning the CFD modelling of confined hydrogen releases

H.O. Kone, Audrey Duclos, Christophe Proust, Franck Verbecke

SOME ISSUES CONCERNING THE CFD MODELLING OF CONFINED HYDROGEN RELEASES

Kone, H.O.[1], Duclos, A.[3] , Proust, C.[1,2]and Verbecke, F.[3]

[1] Sorbonne Universities, UTC-TIMR, 1 rue Dr Schweitzer, Compiègne, 60200, France, habib_kone@yahoo.fr (christophe.proust@utc.fr)
[2] INERIS, PHDS, Parc tech. ALATA, (P.O.Box 2), Verneuil-en-Halatte, 60550, France, christophe.proust@ineris.fr
[3] AREVA Stockage d'Energie, DRT, Domaine du Petit Arbois, (P.O.Box 71), Aix-en-Provence, 13545, France, audrey.duclos@areva.com, franck.verbecke@areva.com

ABSTRACT

In SUSANA E.U. project a rather broad CFD benchmarking exercise was performed encompassing a number of CFD codes, a diversity of turbulence models... It is concluded that the global agreement is good. But in this particular situation, the experimental data to compare with were known to the modelers. In performing, this exercise, the present authors explored the influence of some modeling choices which may have a significant impact on the results (apart from the traditional convergence testing and mass conservation) especially in the situation where little relevant data are available. The configuration investigated is geometrically simple: a vertical round hydrogen jet in a square box. Nevertheless, modeling aspects like the representation of the source and of the boundary conditions have a rather strong influence on the final results as illustrated in this communication. In other words, the difficulties may not be so much in the intrinsic capabilities of the code (which SUSANA tends to show) but more in the physical representation the modelers have. Even in the specific situation addressed in this communication, although looking simple, it may not be so obvious to grasp correctly the leading physical processes.

1.0 CONTEX AND OBJECTIVES

It is clear for most of the stakeholders of the "hydrogen energy" economy that ensuring the safety of hydrogen objects is a major constrain [1]. Failing in doing so may seriously jeopardize future developments. Because of the specificities of hydrogen [2], many leakage scenarios may degenerate in escalating accidents [3] and the very details of each scenario need to be described, quantified before designing, calculating the mitigation barriers. Explosion risk is certainly the most important.

It would not be possible to cover all possible scenarios by experiments and simulations tools are required. CFD modelling is certainly an option but the various benchmarking exercises performed so far [4, 5, 6] indicate that their use might not be so straightforward especially for explosions but also for gas dispersion.

On this aspect (CFD modelling applied to hydrogen leakages cloud formation), a rather broad CFD benchmarking exercise was performed recently (E.U. SUSANA-[7]) encompassing a number of CFD codes, a diversity of turbulence models... It is concluded that the global agreement is good. But in this particular situation, the experimental data to compare with were known to the modellers and the modellers themselves are highly skilled both in numerics and in the various physical aspects pertaining to the problems they simulated.

In performing this exercise, the present authors investigate more specifically in which traps standard safety engineer may fall in when performing CFD simulations. They explored the influence of some modelling choices which may have a significant impact on the results (apart from the traditional

convergence testing and mass conservation) especially in the situation where little relevant data are available.

1.0 EXPERIMENTAL CONFIGURATION AND RESULTS

1.1 Experimental system

The experimental configuration is that used during the DIMITRHY project in France and the experimental campaign is referred to as GAMELAN test series [8]. The objective of this experimental campaign was to investigate further the formation of a flammable atmosphere in a confinement following a leakage of hydrogen.

The device (figure 1) is a 1.26 m high parallelepiped with a 0.93m × 0.93m square section. A 90cm wide and 18 cm high vent is located on a side wall at the top of the box. Helium is injected into the chamber via an injection tube pointing upwards at 210 mm from the bottom of the box. The axis of the injection is the same than that of the box. Helium concentration sensors (catharometers) were placed on three vertical masts (M1, M2 and M4). All are located off the axis of the injection. The details of the arrangement are given on figure 1.

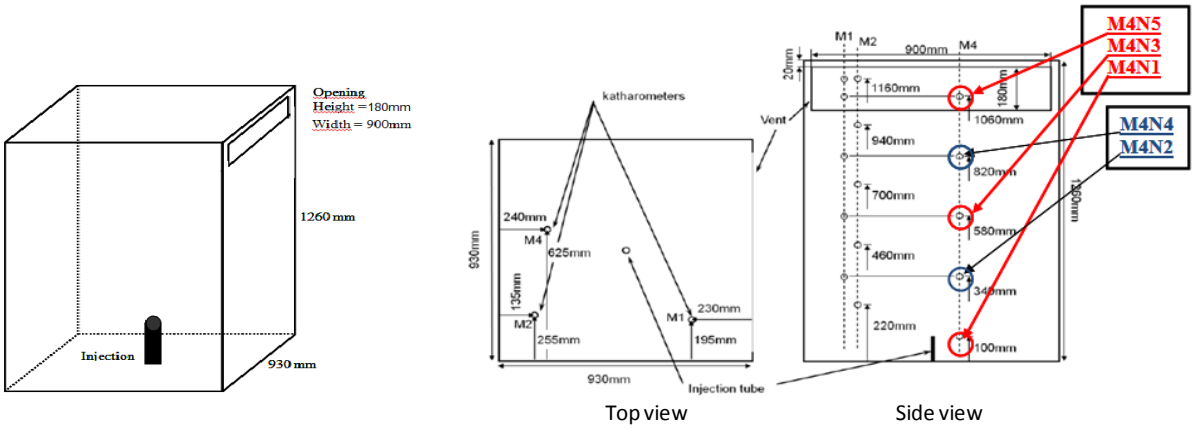

Figure 1 : experimental sketch (left) and sensor arrangement (the labelling of the sensors is MiNj where "i" is mast number and "j" is the number of the sensor with j increasing from the bottom to the top of the enclosure : the labels of the sensors of mast 4 are given)

1.2 Experimental data

A number of situations were investigated by the experimentalists but for the present purpose, only two were selected.

Again helium is injected and not hydrogen. The release and mixing are performed at standard conditions. Only the flowrate and momentum change. In the first test the flowrate is 10 Nl/mn through a 20 mm injection port and in the second one the flowrate is only 180 Nl/mn through a 5 mm orifice.

The experimental results for the mast4 are presented in figure 2 and 3. A homogeneous mixture is obtained for the larger flowrate and a stratified one for the smaller flowrate.

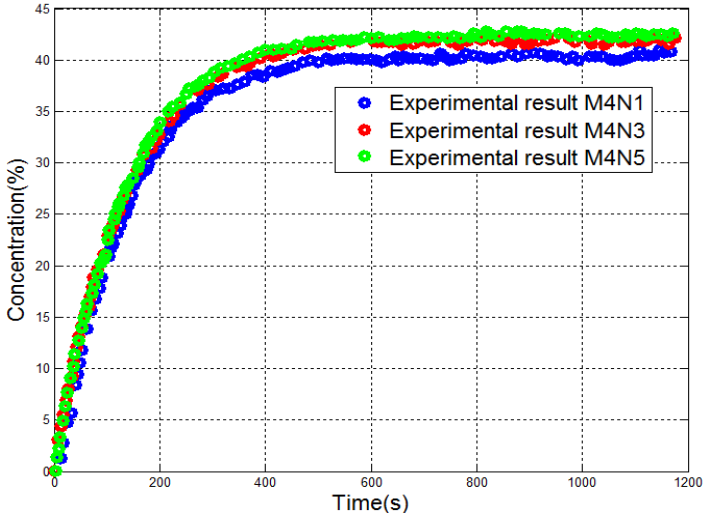

Figure 2: Volumetric concentrations of helium measured on mast 4 (180Nl/min)

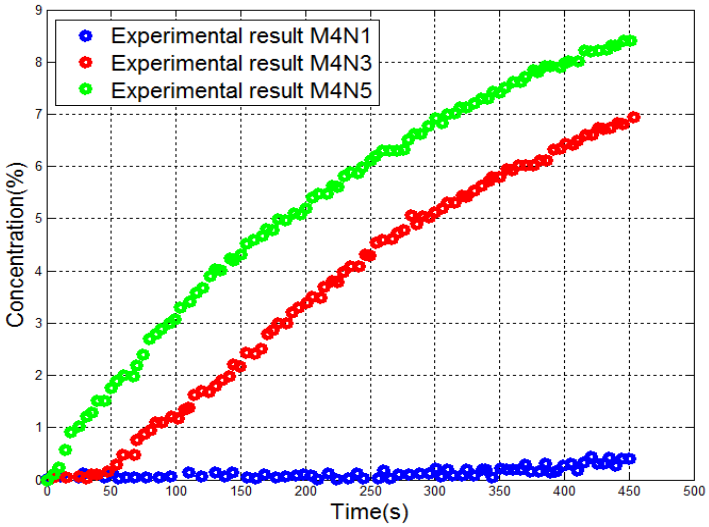

Figure 3: Volumetric concentrations of helium measure on mast4 (10Nl/min)

2.0 SIMULATION CODE AND RESULTS

2.1 Simulation conditions

The simulations were performed using a multipurpose homemade CFD code : MERLIN. MERLIN is a CFD toolbox designed to choose, develop and check the performances of various modelling options proposed in CFD [10]. It is currently being used to investigate the influence of the mesh (regular, unstructured,...), of the numerical solver (about ten are available), turbulence and combustion models within the scope of explosion risks. The code was successfully used in SUSANA project [11]. It is coded using MATHLAB and is capable of performing parallelized calculations on a HPC platform [12].

For this work, an uRANS modelling was chosen using k-epsilon modelling with the buoyancy terms incorporated both in the conservation equations and in the turbulence equations. Both the standard k-epsilon model incorporating a wall function was used but also an alternative model incorporating a modified version of the k-epsilon equation at the wall name “low-Reynolds k-epsilon”.

The general equations of the standard k-epsilon model as used in the present work are recalled in table 1.

Table 1 : Equations of the standard k-epsilon model

Parameter	Description
Mass (ρ density)	$$\frac{\partial \bar{\rho}}{\partial t}+\frac{\partial \bar{\rho}\tilde{u}}{\partial x}+\frac{\partial \bar{\rho}\tilde{v}}{\partial y}+\frac{\partial \bar{\rho}\tilde{w}}{\partial z}=0$$
Momentum (ρ.u) along x	$$\frac{\partial \bar{\rho}\tilde{u}}{\partial t}+\frac{\partial \bar{\rho}\widetilde{u^2}}{\partial x}+\frac{\partial \bar{\rho}\tilde{u}\tilde{v}}{\partial y}+\frac{\partial \bar{\rho}\tilde{u}\tilde{w}}{\partial z}=-\frac{\partial \bar{P}}{\partial x}+(\mu_l+\mu_t)\left[\frac{\partial^2\tilde{u}}{\partial x^2}+\frac{\partial^2\tilde{u}}{\partial y^2}+\frac{\partial^2\tilde{u}}{\partial z^2}\right]$$
Momentum (ρ.v) along y	$$\frac{\partial \bar{\rho}\tilde{v}}{\partial t}+\frac{\partial \bar{\rho}\tilde{u}\tilde{v}}{\partial x}+\frac{\partial \bar{\rho}\widetilde{v^2}}{\partial y}+\frac{\partial \bar{\rho}\tilde{v}\tilde{w}}{\partial z}=-\frac{\partial \bar{P}}{\partial y}+(\mu_l+\mu_t)\left[\frac{\partial^2\tilde{v}}{\partial x^2}+\frac{\partial^2\tilde{v}}{\partial y^2}+\frac{\partial^2\tilde{v}}{\partial z^2}\right]$$
Momentum (ρ.w) along z (height)	$$\frac{\partial \bar{\rho}\tilde{w}}{\partial t}+\frac{\partial \bar{\rho}\tilde{u}\tilde{w}}{\partial x}+\frac{\partial \bar{\rho}\tilde{v}\tilde{w}}{\partial y}+\frac{\partial \bar{\rho}\widetilde{w^2}}{\partial z}=-\frac{\partial \bar{P}}{\partial z}+(\mu_l+\mu_t)\left[\frac{\partial^2\tilde{w}}{\partial x^2}+\frac{\partial^2\tilde{w}}{\partial y^2}+\frac{\partial^2\tilde{w}}{\partial z^2}\right]+\rho\cdot g\frac{(\rho-\rho_a)}{\rho}$$
Species (C: helium conc..)	$$\frac{\partial \bar{\rho}\tilde{C}}{\partial t}+\frac{\partial \bar{\rho}\tilde{u}\tilde{C}}{\partial x}+\frac{\partial \bar{\rho}\tilde{v}\tilde{C}}{\partial y}+\frac{\partial \bar{\rho}\tilde{w}\tilde{C}}{\partial z}=\frac{\partial}{\partial x}\left[\left(\bar{\rho}D_l+\frac{\mu_t}{Sc_t}\right)\frac{\partial\tilde{C}}{\partial x}\right]+\frac{\partial}{\partial y}\left[\left(\bar{\rho}D_l+\frac{\mu_t}{Sc_t}\right)\frac{\partial\tilde{C}}{\partial y}\right]+\frac{\partial}{\partial z}\left[\left(\bar{\rho}D_l+\frac{\mu_t}{Sc_t}\right)\frac{\partial\tilde{C}}{\partial z}\right]$$
Turbulent energy (k)	$$\frac{\partial(\bar{\rho}k)}{\partial t}+\frac{\partial \bar{\rho}\tilde{u}k}{\partial x}+\frac{\partial \bar{\rho}\tilde{v}k}{\partial y}+\frac{\partial \bar{\rho}\tilde{w}k}{\partial z}=\frac{\partial}{\partial x}\left[\left(\mu_l+\frac{\mu_t}{\sigma_k}\right)\frac{\partial k}{\partial x}\right]+\frac{\partial}{\partial y}\left[\left(\mu_l+\frac{\mu_t}{\sigma_k}\right)\frac{\partial k}{\partial y}\right]+\frac{\partial}{\partial z}\left[\left(\mu_l+\frac{\mu_t}{\sigma_k}\right)\frac{\partial k}{\partial z}\right]+R_k+R_b+\bar{\rho}\varepsilon$$
Turbulent dissipation (ε)	$$\frac{\partial \bar{\rho}\varepsilon}{\partial t}+\frac{\partial \bar{\rho}\tilde{u}\varepsilon}{\partial x}+\frac{\partial \bar{\rho}\tilde{v}\varepsilon}{\partial y}+\frac{\partial \bar{\rho}\tilde{w}\varepsilon}{\partial z}=\frac{\partial}{\partial x}\left[\left(\mu_l+\frac{\mu_t}{\sigma_k}\right)\frac{\partial\varepsilon}{\partial x}\right]+\frac{\partial}{\partial y}\left[\left(\mu_l+\frac{\mu_t}{\sigma_k}\right)\frac{\partial\varepsilon}{\partial y}\right]++\frac{\partial}{\partial z}\left[\left(\mu_l+\frac{\mu_t}{\sigma_k}\right)\frac{\partial\varepsilon}{\partial z}\right]+C_{\varepsilon 1}\frac{\varepsilon}{k}(R_k+C_{3\varepsilon}R_b)-C_{\varepsilon 2}\bar{\rho}\frac{\varepsilon^2}{k}$$
Production terms	$$R_k=-\frac{2}{3}\bar{\rho}k\left(\frac{\partial\tilde{u}}{\partial x}+\frac{\partial\tilde{v}}{\partial y}+\frac{\partial\tilde{w}}{\partial z}\right)+\frac{2\mu_t}{3}\left(\frac{\partial\tilde{u}}{\partial x}\right)^2+\frac{2\mu_t}{3}\left(\frac{\partial\tilde{v}}{\partial y}\right)^2+\frac{2\mu_t}{3}\left(\frac{\partial\tilde{w}}{\partial z}\right)^2+\mu_t\left(\frac{\partial\tilde{u}}{\partial y}+\frac{\partial\tilde{v}}{\partial x}\right)^2+\mu_t\left(\frac{\partial\tilde{u}}{\partial z}+\frac{\partial\tilde{w}}{\partial x}\right)^2+\mu_t\left(\frac{\partial\tilde{v}}{\partial z}+\frac{\partial\tilde{w}}{\partial y}\right)^2$$ $$R_b=-\frac{\mu_t}{\rho Sc_t}g\nabla\rho$$
Turbulent viscosity μ_t	$$\mu_t=C_\mu\bar{\rho}\frac{k^2}{\varepsilon}$$
Constants	$$C_\mu=0.09 \quad C_{\varepsilon 1}=1.44 \quad C_{\varepsilon 2}=1.92$$

u, v, w are the mean flow velocities and t the time. P_k is the production term of turbulence due to mean velocity gradients and P_b the production term of turbulence due to buoyancy forces. When the stratification is unstable, P_b is positive and increases k and when the stratification is stable this number becomes negative and contributes to the reduction of the turbulent kinetic energy. μ_l (D_l) is the molecular viscosity (diffusivity), usually neglected. The specific mass of the mixture is a linear function of the molar fraction of the constituents (air and helium). The turbulent Schmidt number, Sct, is set to 0.7. The turbulent Prandtl numbers for k and ε are respectively σ_k and σ_ε and are equal to 1.

Coefficient $C_{3\varepsilon}$ which represents the influence of the buoyancy in the turbulent dissipation term is modeled as follow:

$$C_{3\varepsilon}=\tanh\frac{u_{g\perp}}{u_{g\parallel}} \qquad [1]$$

where $u_{g\perp}$ represents the velocity component perpendicular to the force of gravity and $u_{g\parallel}$ the velocity component parallel to the force of gravity.

As known, the k-Ɛ model is valid far from wall boundaries. In the boundary layers flows, the model does not provide a correct damping for the turbulent parameters and the wrong velocity profiles are predicted together with far too much turbulence. To overcome this difficulty, the solutions for k, ε and u (if u is the velocity component parallel to the wall) are calculated using analytic functions issued from boundary layers theories:

$$y^+ = \frac{y \cdot \tau_w}{\nu_l};\ u_\tau = \sqrt{\frac{\tau_w}{\rho}};\ u^+ = \frac{U}{u_\tau} = \frac{1}{k}\ln(E \cdot y^+);\ k = \frac{u_\tau^2}{\sqrt{C_\mu}};\ \varepsilon = \frac{u_\tau^3}{\kappa y};\ \tau_w = \mu_l \frac{\partial U}{\partial y}|_{y=0}$$

where τ_w is the shear stress at the boundary, ν_l the laminar kinetic viscosity, E=9.8 and κ=0.41. This expression is used up to a distance from the wall such that y+=500. Because of the form of the equation, this model is sometimes referred to as the log-law.

An alternative consists in using the "low Reynolds number k-epsilon" model incorporating an asymptotic approximation of the k-epsilon model in the boundary layer near the walls. The modified equations are only those of k and epsilon and are shown in table 2.

Table 2 : Equations of the "low Reynolds number" k-epsilon model

Parameter	Description
Turbulent energy (k)	$\frac{\partial(\bar{\rho}k)}{\partial t} + \frac{\partial \bar{\rho}\tilde{u}k}{\partial x} + \frac{\partial \bar{\rho}\tilde{v}k}{\partial y} + \frac{\partial \bar{\rho}\tilde{w}k}{\partial z} = \frac{\partial}{\partial x}\left[\left(\mu_l + \frac{\mu_t}{\sigma_k}\right)\frac{\partial k}{\partial x}\right] + \frac{\partial}{\partial y}\left[\left(\mu_l + \frac{\mu_t}{\sigma_k}\right)\frac{\partial k}{\partial y}\right] + \frac{\partial}{\partial z}\left[\left(\mu_l + \frac{\mu_t}{\sigma_k}\right)\frac{\partial k}{\partial z}\right] + R_k + R_b + \bar{\rho}\varepsilon^* - D$
Modified turbulent dissipation (ε*)	$\frac{\partial \bar{\rho}\varepsilon^*}{\partial t} + \frac{\partial \bar{\rho}\tilde{u}\varepsilon^*}{\partial x} + \frac{\partial \bar{\rho}\tilde{v}\varepsilon^*}{\partial y} + \frac{\partial \bar{\rho}\tilde{w}\varepsilon^*}{\partial z} = \frac{\partial}{\partial x}\left[\left(\mu_l + \frac{\mu_t}{\sigma_k}\right)\frac{\partial \varepsilon^*}{\partial x}\right] + \frac{\partial}{\partial y}\left[\left(\mu_l + \frac{\mu_t}{\sigma_k}\right)\frac{\partial \varepsilon^*}{\partial y}\right] + + \frac{\partial}{\partial z}\left[\left(\mu_l + \frac{\mu_t}{\sigma_k}\right)\frac{\partial \varepsilon^*}{\partial z}\right] + C_{\varepsilon 1}\frac{\varepsilon^*}{k}(R_k + C_{3\varepsilon}R_b) - C_{\varepsilon 2}f_2\bar{\rho}\frac{\varepsilon^{*2}}{k} + E$
ε*	$\varepsilon^* = \varepsilon - 2\nu\left(\frac{\partial k^{\frac{1}{2}}}{\partial y}\right)^2$
D and E	$D = \bar{\rho}\varepsilon - \bar{\rho}\varepsilon^* \qquad E = 2\frac{\mu_l \mu_t}{\bar{\rho}}\left(\frac{\partial^2 u_i}{\partial x_j \partial x_k}\right)\left(\frac{\partial^2 u_i}{\partial x_j \partial x_k}\right)$
Species (C: helium conc..)	$\frac{\partial \bar{\rho}\tilde{C}}{\partial t} + \frac{\partial \bar{\rho}\tilde{u}\tilde{C}}{\partial x} + \frac{\partial \bar{\rho}\tilde{v}\tilde{C}}{\partial y} + \frac{\partial \bar{\rho}\tilde{w}\tilde{C}}{\partial z} = \frac{\partial}{\partial x}\left[\left(\bar{\rho}D_l + \frac{\mu_t}{Sc_t}\right)\frac{\partial \tilde{C}}{\partial x}\right] + \frac{\partial}{\partial y}\left[\left(\bar{\rho}D_l + \frac{\mu_t}{Sc_t}\right)\frac{\partial \tilde{C}}{\partial y}\right] + \frac{\partial}{\partial z}\left[\left(\bar{\rho}D_l + \frac{\mu_t}{Sc_t}\right)\frac{\partial \tilde{C}}{\partial z}\right]$
Turbulent viscosity μ_t	$\mu_t = C_\mu f_\mu \bar{\rho}\frac{k^2}{\varepsilon}$ ...with .... $f_\mu = \exp\left(\frac{-2.5}{1 + \frac{R_t}{50}}\right)$ ....and ..... $R_t = \frac{k^2}{\nu\varepsilon}$
Damping factor f_2	$f_2 = 1 - 0.3\exp(-R_t^2)$

Two damping terms appear, f_2 and f_μ: f_2 considers the effects of the low local Reynolds number near the boundary, which contributes to the growth of Ɛ in this zone; f_μ intervenes in the calculation of μ_t(turbulent viscosity) is a damping function permitting to quickly decrease the turbulent viscosity in the zone of near boundary. It is a logical extension of the standard k-epsilon model and shares many of its advantages, but uses more memory.

The initial and boundary conditions are provided in table 3. Remember that in RANS simulations some turbulence is always present and is fitted with the mean velocity field. Some non zero initial values of k and epsilon have to be then to be settled. Their relevancy is not of primary importance since the calculations will rapidly provide the equilibrium value. In all zones, a weak turbulence level was chosen assuming the turbulent viscosity will be equal to the molecular viscosity with provides the following values for k and epsilon : $k=0.0001xU^2$ and $epsilon=0.0001xU^4$ where U is the local mean velocity. When U is zero k and epsilon are set to 0.0001.

Table 3 : initial and boundary conditions

Location	Conditions
vent	atmospheric pressure, only normal velocity
injection	atmospheric pressure, mass flowrate constant, helium volume fraction=1
enclosure	atmospheric pressure, normal velocity at the wall = 0

The numerical resolution involves a Roe solver with the “minmod” limiter for the space discretization of the convective terms, the classical central scheme for the space discretization of the diffusive terms and a fully explicit formulation (one order Euler explicit scheme) for the time derivatives. The numerical solver is therefore second order in space and first order in time. The orientation of the mesh is of secondary importance for slowly convective-diffusive problems and a regular mesh was chosen for its ease of implementation. MERLIN nevertheless offers the possibility to refine the mesh at specific locations. In the present case, refined zone were produced in the plume and in the upper part of the chamber (where some accumulation is possible) following a sort trial and error procedure (AMA for Anisotropic Mesh Adaptation: [13]) which ensures the refinement zone are correctly located. A view of the mesh is shown on figure 4 and the various mesh densities tested are presented in table 4.

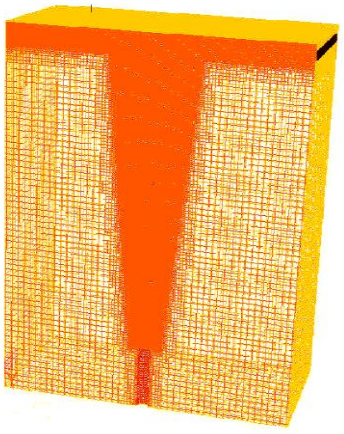

Figure 4: Mesh used to simulate Gamelan experiments

Table 4 : mesh refinements tested

Meshes	Number of cells in the plume and upper part of the enclosure	Number of cells in the other parts of the chamber	Number of cells in the injection port (across the diameter)	Total number of cells
Mesh1	544214	625420	5	1169634
Mesh2	2825314	3325712	12	6151026
Mesh3	5555000	6533644	20	12088644
Mesh4	6514312	7630255	24	14144567

Apart from the standard consistency checks, the sensitivity to the mesh was tested on the larger flowrate case (figure 5). Convergence is obtained with mesh 3 and 4 meaning a cell size of about 3 mm in the plume and top of the vessel and 5 mm elsewhere.

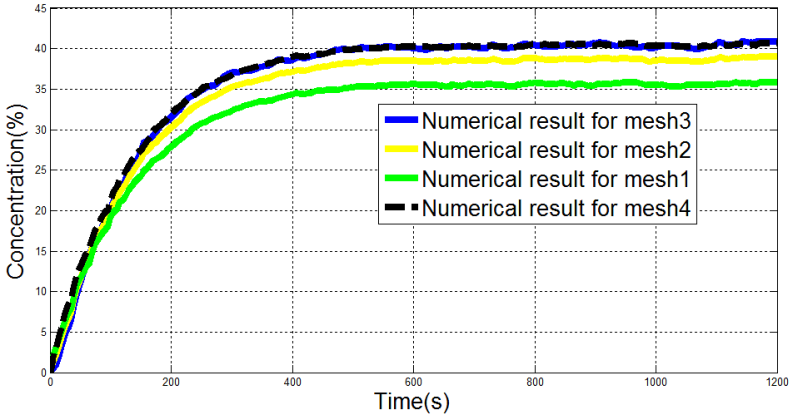

Figure 5: numerical results with the different meshes: mast 4 (M4N1), 180 Nl/min

The simulations were performed with mesh 3 but note that a rapid degradation of the accuracy can appear when the mesh size is not small enough.

2.2 Results

A typical sequence representing the evolution of the mixture is presented in figure 6 with the standard k-epsilon model.

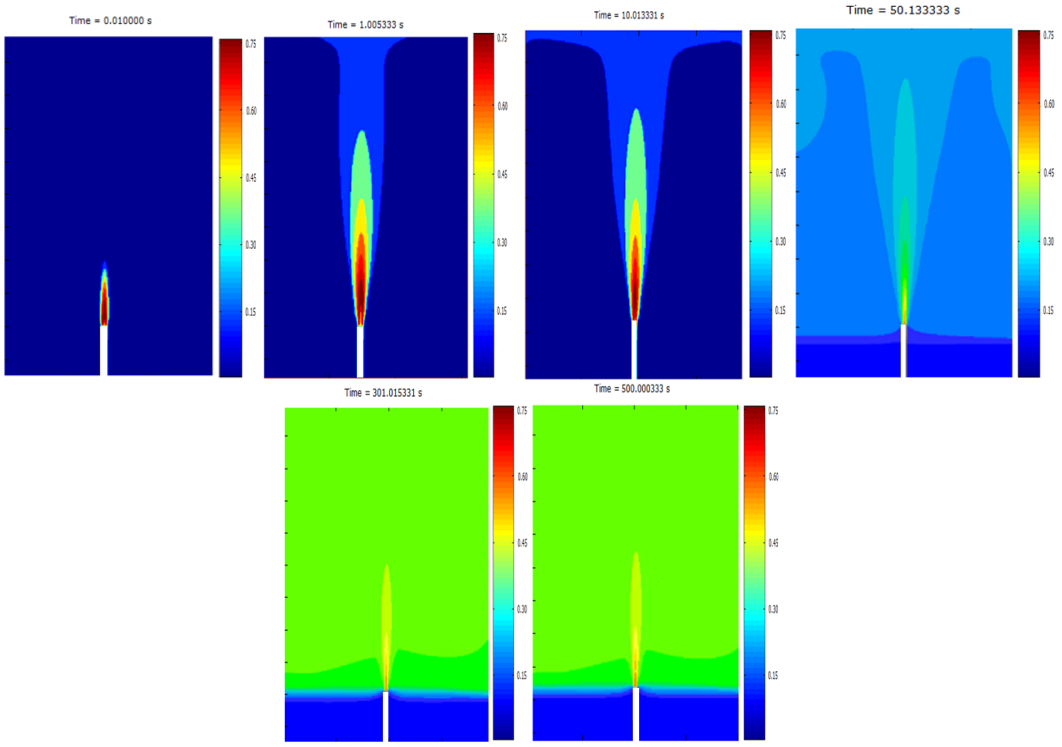

Figure 6: Volumetric concentration of helium at different times in the symmetry plane for 180 Nl/mn : standard k-epsilon model

An extraction of the concentration of helium for the location of the sensors on mast 4 is presented in figure 7 and should be compared to the experimental results figure 2.

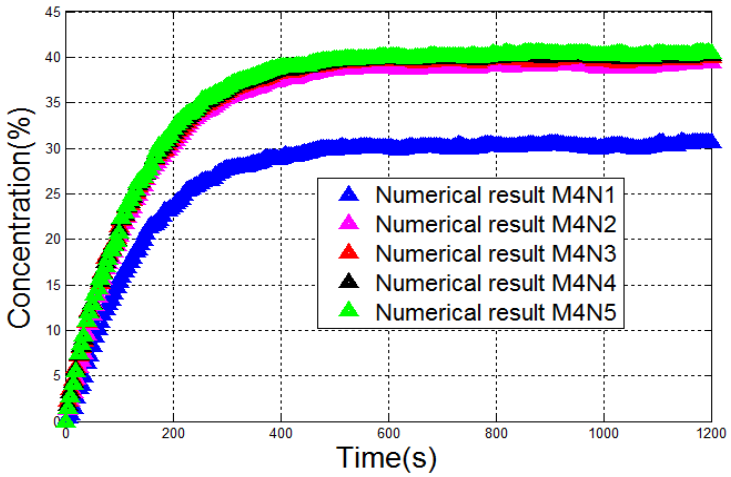

Figure 7 : Volumetric concentrations of helium calculated for mast 4 (180Nl/min) and the standard k-epsilon model

The simulated volumetric concentration on the upper “sensors” is closed to that measured. But some stratification is calculated (-10%) whereas in the experiment, the mixture is perfectly homogeneous.

The results for the second experiment (10 Nl/mn) are shown on figure 8 (simulations and measurements superposed). In this case, the discrepancies are very large both in trends and in absolute values suggesting the physics is not well taken into account.

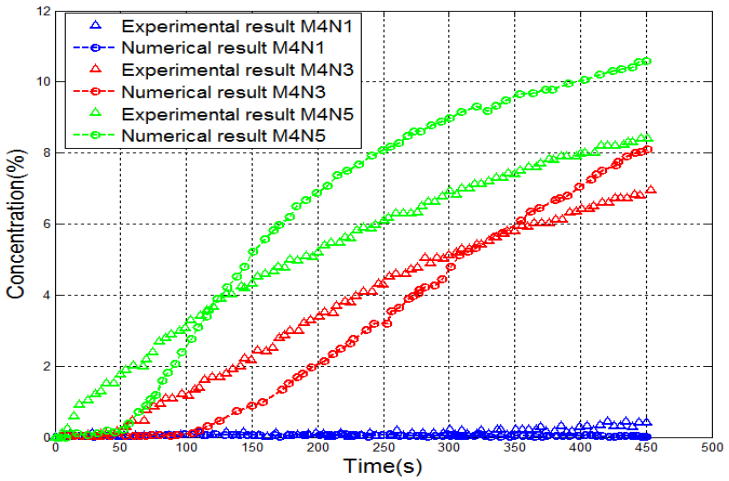

Figure 8 : Volumetric concentrations of helium calculated for mast 4 (10Nl/min) and the standard k-epsilon model

Nonetheless, the uRANS formulation in general and the k-epsilon model in particular should perform correctly in this situation. A deeper analysis is required concerning the flow. Non dimensional numbers can be used and in particular the Reynolds numbers comparing the inertial and viscosity forces and the Froude numbers comparing the inertial to the buoyancy forces. Two flows need to be considered : that issued from the injection and that occurring along the boundaries of the enclosure. To calculate the Reynolds and Froude numbers of the enclosure a convective flow velocity should be estimated. It is basically that of the plume impinging on the top of the enclosure and could be estimated assuming the momentum is preserved from the injection point to the top (to estimate the convective velocity the buoyancy forces are ignored). The final expressions are provided in table 5.

Table 5 : Estimation of the non dimensional flow numbers

Flowrate (Nl/mn)	Reynolds number of the injection $\mathrm{Re} = \frac{\rho_{He} \cdot U_{orifice} \cdot D_{orifice}}{\mu_{He}}$	Froude number of the injection $Fr = \frac{\sqrt{\rho_{He}} \cdot U_{orifice}}{\sqrt{g \cdot D_{orifice} \cdot (\rho_{air} - \rho_{He})}}$	Reynolds number of the enclosure $\mathrm{Re} = \sqrt{\frac{\rho_{air}}{\rho_{He}}} \cdot \mathrm{Re}_{orifice}$	Froude number of the enclosure $Fr = \frac{\sqrt{\rho_{He}} \cdot D_{orifice} \cdot U_{orifice}}{\sqrt{g \cdot V_{enclosure} \cdot (\rho_{air} - \rho_{He})}}$
10	100	0.45	260	0.001
180	6500	280	17500	0.1

Clearly, the buoyancy forces play an important role especially at the lower flowrate. In this situation even, the Reynolds numbers are all small suggesting the boundary layers may not be fully developed as implicitly assumed when using the log laws at the walls in the standard k-epsilon model.

Because of this, the low Reynolds number k-epsilon was used and the calculations run again. the results are presented on figures 9 and 10. The agreement is now excellent.

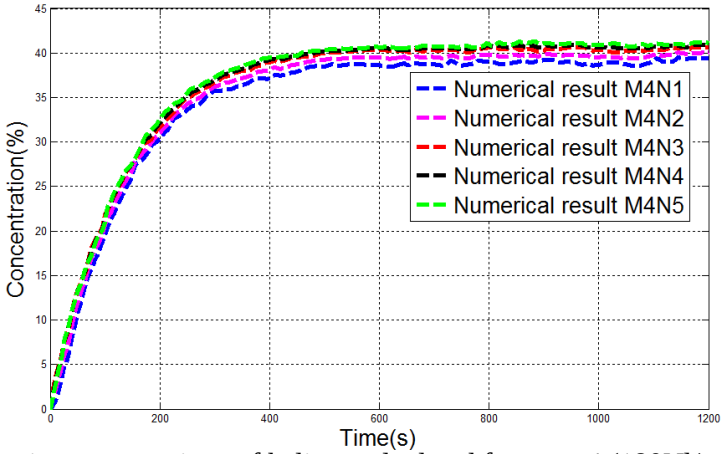

Figure 9 : Volumetric concentrations of helium calculated for mast 4 (180Nl/min) and the low Reynolds k-epsilon model

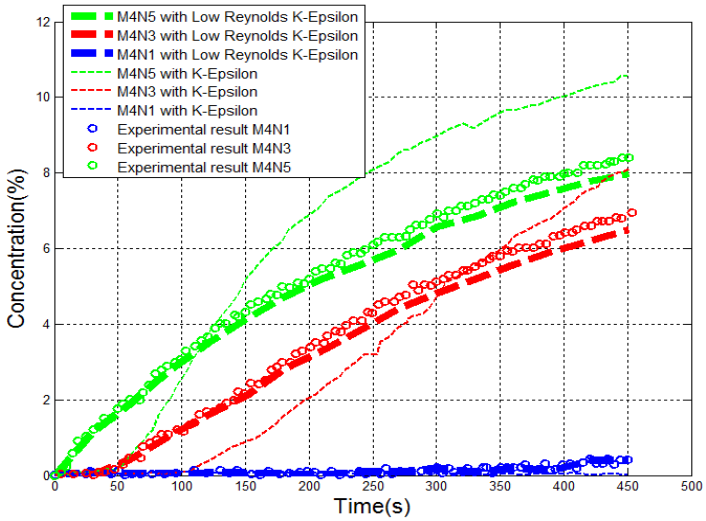

Figure 10 : Volumetric concentrations of helium calculated for mast 4 (10Nl/min) and the low Reynolds k-epsilon model

3.0 DISCUSSION AND CONCLUSION

Somewhat surprisingly for the present authors, even in these rather simple looking situations, obtaining a satisfactory estimation may be a challenging task. The good news may be that the choice of the numerical scheme and of the mesh topology seem of secondary importance contrary to what is observed for shock waves for instance.

Here the choice of the physical models is a key point. Using a standard well established k-ε model, even provided with a standard log-law for the boundary walls, could ill estimate the concentration/size of the explosive by a factor of about 30% which is considerable as far as the potential subsequent explosion effects are concerned.

Quite a significant amount of structured knowledge (not only a culture of…) in fluid mechanics was required to find the reason for the discrepancy and the latter was identified only after consideration of the experimental results. So the confrontation with existing data is certainly desired but looking for the relevant experiments containing the relevant key physics (with regard to the practical situation to be studied) remains very challenging since a rather deep knowledge of the physics is compulsory. The user dimension is then particularly questioned, not the capabilities of the codes.

A specific aspect concerns the boundary layers. They are everywhere in practical situations and the present illustration shows that a wrong physical representation of them may lead to severe mismatches.

A further point pertains to the size of the computational cells and to the "cost" of the simulations. As shown with this example, although geometrically simple, the cell size needs to be small enough to resolve correctly the formation of the layer. The convergence in "mesh" was reached with about 10^7 cells and the CPU time for such a calculation is typically a week long. The time required for choosing the modeling options and for the convergence testing may require at least 2 weeks more if done properly. The present work suggests that the accuracy is likely to drop extremely fast when "coarsening" the cells size. For instance a decrease of only 20% in the number of cells (increase of 10% cell size) results in a drop of 5 to 10% in accuracy.

So performing reasonable simulations may be long and thus expensive. In safety practice, the simulation of the cloud characteristics is only a brick and the code user may wish to reduce the calculation time to investigate more scenarios. The user needs absolutely be aware that totally wrong conclusions may be obtained… Perhaps, additional modeling options need to be provided to safety engineer for instance to bound the risk scenarios to be addressed at a later step by CFD or to obtain trends and reference values.

4.0 REFERENCES

1. Edwards, P. P., Kutnetsov, V. L., David, W. I. F., Hydrogen Energy , *Phil. Trans. R. Soc. A*, **365**, 2007, pp. 1043–1056
2. Crowl, D.A., Jo, Y.D., The hazards and risks of hydrogen, *Journal of Loss Prevention in the Process Industries*, **20**, 2007, pp. 158–164
3. Galassi, M.C., Papanikolaou, E., Baraldi, D., Funnemark, E., Håland, E., Engebø, A., Haugom, G.P., Jordan, J., HIAD – hydrogen incident and accident database, *International Journal of Hydrogen Energy*, **37**, 2012, pp. 17351–17357
4. Venetsanos, A.G., Papanikolaou, E., Delichatsios, M., Garcia, J., Hansen, O.R., Heitsch, M., Huser, A., Jahn, W., Jordan, T., Lacome, J.-M., Ledin, H.S., Makarov, D., Middha, P., Studer, E., An inter-comparison exercise on the capabilities of CFD models to predict the short and long term distribution and mixing of hydrogen in a garage, *International Journal of Hydrogen Energy*, **34**, 2009, pp. 5912–5923
5. Molkov, V., Shentsov., V., Numerical and physical requirements to simulation of gas release and dispersion in an enclosure with one vent, *International Journal of Hydrogen Energy*, **39**, 2014, pp. 13328–13345
6. Baraldi, D., Kotchourko, A., Lelyakin, A., Yanez, J., Gavrikov, A., Efimenko, A., Verbecke, F., Makarov, D., Molkov, V., Teodorczyk, A., An inter-comparison exercise on CFD model capabilities to simulate hydrogen deflagrations with pressure relief vents, , *International Journal of Hydrogen Energy*, **35**, 2014, pp. 12381–12390
7. SUSANA project, SUpport to SAfety ANalysis of Hydrogen and Fuel Cell Technologies, E.U. funded project FP7-JTI, ID325386
8. Cariteau, B., Tkatschenko, I., Experimental Study of the Effects of Vent Geometry on the Dispersion of a Buoyant Gas in a Small Enclosure, *International Journal of Hydrogen Energy*, **38**, 2013, pp. 8030–38
9. Kone, H.O., Simulating large scale (industrial) explosions using Computational Fluid Dynamics (CFD): Studying modeling strategies with MERLIN a CFD toolbox, *PhD thesis memory*, Sorbonne Universities, Technological University of Compiègne, 2017, France.
10. Giannissi, S., Tolias, I., Venetsanos, A., Melideo, D., Baraldi, D., Shentsov, V., Makarov, D., Molkov, V., Slater, S., Kotchourko, K., Ren, K., Duclos, A., Verbecke, F., Report on model benchmarking exercise 2, *SUSANA deliverable*, **D.5.3**, 2016.
11. https://pilcam2.wikispaces.com/

12. Alauzet, F., Frey, P.J., Mohammadi, B., Anisotropic mesh adaptation. Applications to transient CFD problems, Computational Fluid and Solid Mechanics, 2003, pp. 1851-1854